

# Three-Dimensional Static Modeling of the Lumbar Spine

Ernur Karadogan

Robert L. Williams II<sup>1</sup>

Mechanical Engineering Department,  
Ohio University,  
Athens, OH 45701-2979

*This paper presents three-dimensional static modeling of the human lumbar spine to be used in the formation of anatomically-correct movement patterns for a fully cable-actuated robotic lumbar spine which can mimic in vivo human lumbar spine movements to provide better hands-on training for medical students. The mathematical model incorporates five lumbar vertebrae between the first lumbar vertebra and the sacrum, with dimensions of an average adult human spine. The vertebrae are connected to each other by elastic elements, torsional springs and a spherical joint located at the inferoposterior corner in the mid-sagittal plane of the vertebral body. Elastic elements represent the ligaments that surround the facet joints and the torsional springs represent the collective effect of intervertebral disc which plays a major role in balancing torsional load during upper body motion and the remaining ligaments that support the spinal column. The elastic elements and torsional springs are considered to be nonlinear. The nonlinear stiffness constants for six motion types were solved using a multiobjective optimization technique. The quantitative comparison between the angles of rotations predicted by the proposed model and in the experimental data confirmed that the model yields angles of rotation close to the experimental data. The main contribution is that the new model can be used for all motions while the experimental data was only obtained at discrete measurement points. [DOI: 10.1115/1.4007172]*

*Keywords: human lumbar spine, three-dimensional static modeling, robotic lumbar spine, RLS*

## 1 Introduction

The art of palpation is usually taught by using human patients who are palpated by the instructor for demonstrative purposes. Medical students watch the process and palpate each other, generally with limited dysfunctions. It is difficult to find and demonstrate patients for every dysfunction taught. There exists no assessment device to objectively evaluate clinical palpation of students. To enhance palpation teaching assessment, a cable-actuated robotic lumbar spine (RLS) is currently under development [1]. The current study involves lumbar spine movement patterns to define RLS motions under different loading conditions.

Studies for mathematical modeling of the thoracic, lumbar and thoracolumbar spine include [2–12]. Reference [8] developed the first static 3D model for spine nonlinear force analysis. The authors used a stiffness method considering the vertebrae as rigid bodies connected with deformable elements having axial, torsional, bending and shear resistance. In a continuation [9], the authors emphasized the kinematic constraints role of facet joints. Facets and the ligaments carry loads in bending and torsion [10] performed a lumbar spine static simulation based on experimental data in Ref. [11]. They simulated ligamentous and nonligamentous soft tissue using linear springs, whereas nonlinear behavior

is expected [12] used a L3-L4 segment finite element model to analyze the facet orientation sensitivity and the initial joint gap between facets. Both parameters affected the facet load.

In this paper, a model of the human lumbar spine using nonlinear elastic elements and torsional springs based on experimental data is proposed. The purpose is to create a model that accurately estimates the movement patterns of the lumbar vertebrae under externally-applied forces and moments. The experimental data used presents vertebral motion at discrete values. The proposed model estimates movement patterns continuously, i.e., for any applied moment. The model's validation and simulation results are presented.

## 2 Methods

**2.1 Construction of the Lumbar Spine Geometry.** The lumbar spine geometry has average human dimensions based on experimental data [1]. All geometry parameters have been previously used in the literature, except for the facet plane and facet plane angle. Assuming sagittal symmetry, we define a facet plane that connects the four facet centers. This plane allows the attachment of posterior elements with various dimensions, making the system modular. The facet plane angle is the angle between the facet plane and the vertebral body posterior wall. A cylindrical shape is assumed for vertebral bodies. Figure 1 shows the facet plane angle and cylindrical vertebral body. The lumbar spine geometry is shown in Fig. 2.

**2.2 Mathematical Model.** The mathematical model includes five lumbar vertebrae and the sacrum, ten elastic elements that connect inferior facets of one vertebra to the superior facets of the lower one and 15 torsional springs that represent the collective torque-resisting effects of the intervertebral disc and the ligaments. The significant motion of the vertebrae during spinal movement is rotational [11–13]. Therefore, a spherical joint connects vertebrae. This joint location is critical to provide anatomically-correct motion for each vertebra during overall lumbar movement. The spherical joints are located at the inferoposterior corners of the vertebral bodies because the experimental data used is Ref. [13]. In that reference, the inferoposterior corner of

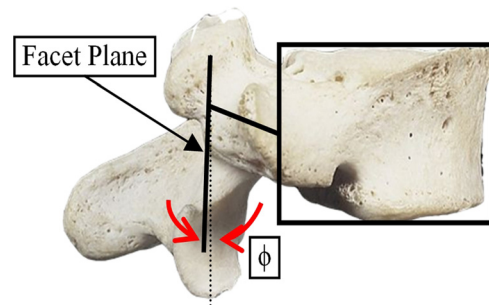


Fig. 1 Facet plane and angle

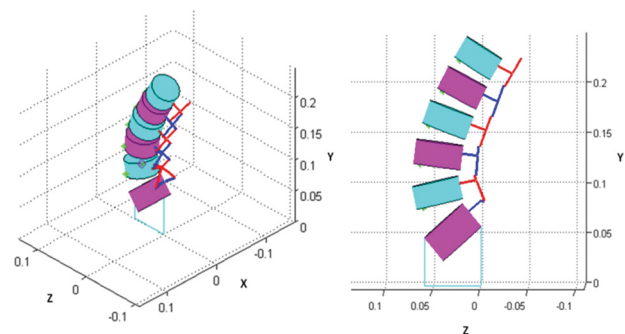
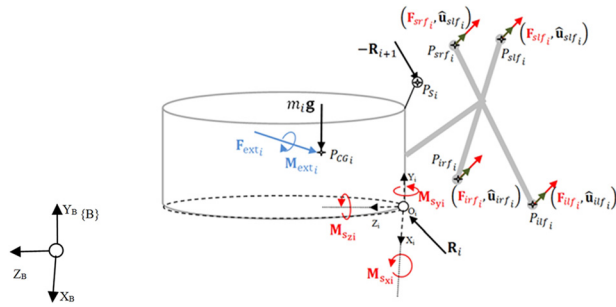


Fig. 2 3D Geometry of the lumbar spine [1]

<sup>1</sup>Corresponding author.

Manuscript received September 14, 2011; final manuscript received July 11, 2012; published online xx xx, xxxx. Assoc. Editor: Michael Sacks.



**Fig. 3 Free-body diagram of a vertebra**

each vertebra is the coordinate frame origin for which the rotation angles were recorded.

The equations of static equilibrium for forces and moments are derived for each vertebra using the free-body diagram (Fig. 3). Force equilibrium in the base frame {B} can be written as:

$$\sum \mathbf{F}_i = m_i \mathbf{g} + \mathbf{F}_{srf_i} + \mathbf{F}_{slfi} + \mathbf{F}_{irfi} + \mathbf{F}_{ilfi} + \mathbf{R}_i - \mathbf{R}_{i+1} = -\mathbf{F}_{ext_i} \quad (1)$$

$m_i$  is the  $i$ -th vertebra mass,  $\mathbf{g} = \{0 -9.81 0\}^T$  is the gravity vector,  $\mathbf{F}_{srf_i}$ ,  $\mathbf{F}_{slfi}$ ,  $\mathbf{F}_{irfi}$ ,  $\mathbf{F}_{ilfi}$  are the forces due to the elastic element connected to the superior right facet, superior left facet, inferior right facet and inferior left facet, and  $\mathbf{R}_i$  is the spherical joint reaction force.  $\mathbf{F}_{ext_i}$  is the external force applied to the  $i$ -th vertebra center of gravity.

As in Ref. [13], the external forces are all zero except for one at the uppermost vertebra L1. This 100-Newton compressive force represents partial torso weight. This external force's line of action passes through the centers of gravity of first lumbar and first sacral vertebra during motion. The elastic elements forces connecting the facets in Eq. (1) are:

$$\begin{aligned} \mathbf{F}_{srf_i} &= {}^i\mathbf{R}(k_{srf_i}(\|{}^i\mathbf{R}^{i+1}\mathbf{P}_{irfi+1} - {}^i\mathbf{P}_{srf_i}\| - G)){}^i\hat{\mathbf{u}}_{srf_i} \\ \mathbf{F}_{slfi} &= {}^i\mathbf{R}(k_{slfi}(\|{}^i\mathbf{R}^{i+1}\mathbf{P}_{ilfi+1} - {}^i\mathbf{P}_{slfi}\| - G)){}^i\hat{\mathbf{u}}_{slfi} \\ \mathbf{F}_{irfi} &= {}^i\mathbf{R}(k_{irfi}(\|{}^i\mathbf{R}^{i-1}\mathbf{P}_{srfi-1} - {}^i\mathbf{P}_{irfi}\| - G)){}^i\hat{\mathbf{u}}_{irfi} \\ \mathbf{F}_{ilfi} &= {}^i\mathbf{R}(k_{ilfi}(\|{}^i\mathbf{R}^{i-1}\mathbf{P}_{slfi-1} - {}^i\mathbf{P}_{ilfi}\| - G)){}^i\hat{\mathbf{u}}_{ilfi} \end{aligned} \quad (2)$$

${}^i\mathbf{R}$  is the rotation matrix giving the orientation of frame {i} with respect to {B}, using X-Y-Z ( $\alpha, \beta, \gamma$ ) Euler angles:

$${}^i\mathbf{R} = \begin{bmatrix} c\beta c\gamma & -c\beta s\gamma & s\beta \\ s\alpha s\beta c\gamma + c\alpha s\gamma & -s\alpha s\beta s\gamma + c\alpha c\gamma & -s\alpha c\beta \\ -c\alpha s\beta c\gamma + s\alpha s\gamma & c\alpha s\beta s\gamma + s\alpha c\gamma & c\alpha c\beta \end{bmatrix} \quad (3)$$

where  $c\alpha = \cos\alpha$ ,  $c\beta = \cos\beta$ ,  $c\gamma = \cos\gamma$ ,  $s\alpha = \sin\alpha$ ,  $s\beta = \sin\beta$ ,  $s\gamma = \sin\gamma$ .

The remaining variables in Eq. (2) are:  $G = 2 \text{ mm}$  [14,15] is the facets joint gap (equal to the unstretched springs length when the lumbar spine is upright),  ${}^i\mathbf{P}_{irfi}$ ,  ${}^i\mathbf{P}_{ilfi}$ ,  ${}^i\mathbf{P}_{srfi}$ ,  ${}^i\mathbf{P}_{slfi}$  are the facet centers position vectors with respect to local vertebral frame {i} (Fig. 3),  $k_{srf}$  is the stiffness constant, and  ${}^i\hat{\mathbf{u}}_{srf_i}$  is the unit vector in the local vertebral frame {i} that defines the force line of action in the corresponding elastic element. The remaining forces and stiffness constants are defined similarly.

The static equilibrium equations for the moments about the local frame {i} are:

$$\begin{aligned} \sum \mathbf{M}_i &= \mathbf{M}_s + ({}^i\mathbf{P}_{CG_i} \times {}^i\mathbf{R} \mathbf{F}_{ext_i}) + ({}^i\mathbf{P}_{CG_i} \times {}^i\mathbf{R} m_i \mathbf{g}) \\ &+ ({}^i\mathbf{P}_{srf_i} \times {}^i\mathbf{R} \mathbf{F}_{srf_i}) + ({}^i\mathbf{P}_{slfi} \times {}^i\mathbf{R} \mathbf{F}_{slfi}) \\ &+ ({}^i\mathbf{P}_{irfi} \times {}^i\mathbf{R} \mathbf{F}_{irfi}) + ({}^i\mathbf{P}_{ilfi} \times {}^i\mathbf{R} \mathbf{F}_{ilfi}) \\ &- ({}^i\mathbf{P}_{S_i} \times {}^i\mathbf{R} \mathbf{R}_{i+1}) \\ &= -{}^i\mathbf{M}_{ext_i} \end{aligned} \quad (4)$$

**Table 1 Experimental load-displacement data for L3-L4 [13]**

	External Moment, $M_{ext}$ (Nm)			Motion (deg)		
	X	Y	Z	X	Y	Z
Flexion	2.50	0.00	0.00	5.00	0.00	0.00
	5.00	0.00	0.00	6.00	0.00	0.00
	7.50	0.00	0.00	6.50	0.00	0.00
	10.00	0.00	0.00	7.00	0.00	0.00
Extension	-2.50	0.00	0.00	-1.50	0.00	0.00
	-5.00	0.00	0.00	-2.25	0.00	0.00
	-7.50	0.00	0.00	-2.00	0.00	0.00
	-10.00	0.00	0.00	-2.75	0.00	0.00
Left Torque	0.00	2.50	0.00	0.75	0.50	0.25
	0.00	5.00	0.00	1.13	1.00	0.38
	0.00	7.50	0.00	1.25	1.63	0.50
	0.00	10.00	0.00	1.75	1.75	0.63
Right Torque	0.00	-2.50	0.00	0.50	-0.88	-0.38
	0.00	-5.00	0.00	-0.25	-1.75	-0.50
	0.00	-7.50	0.00	0.50	-1.88	-0.75
	0.00	-10.00	0.00	0.63	-2.00	-1.00
Right Bending	0.00	0.00	2.50	0.75	0.75	3.10
	0.00	0.00	5.00	1.50	0.80	4.00
	0.00	0.00	7.50	1.75	0.80	4.75
	0.00	0.00	10.00	1.50	1.25	5.00
Left Bending	0.00	0.00	-2.50	-0.25	-0.60	-3.50
	0.00	0.00	-5.00	0.60	-1.00	-4.50
	0.00	0.00	-7.50	1.50	-1.00	-5.00
	0.00	0.00	-10.00	1.40	-1.25	-5.50

${}^i\mathbf{M}_s = \{{}^iM_{sxi} {}^iM_{syi} {}^iM_{szi}\}^T$  is the moment vector due to torsional springs attached to the  $i$ -th vertebra,  ${}^iM_{sxi} = -k_{sxi}q_{xi}$  is the moment due to the torsional spring about the  $x$ -axis,  $k_{sxi}$  is the spring constant of the torsional spring about the  $x$ -axis and  $q_{xi}$  is the angular displacement.  ${}^iM_{syi}$  and  ${}^iM_{szi}$  are the same way as  ${}^iM_{sxi}$  using  $y$ - and  $z$ - axes.  ${}^i\mathbf{P}_{CG}$  and  ${}^i\mathbf{P}_S$  are the position vectors from the local origin to the center of gravity and center of the socket in {i} (Fig. 3).

**2.3 Experimental Data.** The simulation results to validate the proposed model are based on experimental data in Ref. [13]. These researchers used fresh-frozen lumbosacral-spine specimens with only ligamentous soft tissue to test lumbar spine mechanical behavior by constructing load-displacement curves for each vertebra under specific loading conditions. Motion was induced by applying pure moments to the first lumbar vertebra. This moment, applied about one of the three axes of rotation, caused spine to flex/extend, bend or rotate axially. The applied moment magnitude was 2.5, 5.0, 7.5 and 10 Nm. The data contained the translation and rotation of each vertebra under the tested loading condition. It is emphasized once more, however, that the rotational motion remained dominant over the translational motion. A load-displacement data example for L3-L4 segment model validation is in Table 1.

### 3 Results

In the first stage of validation, the nonlinear stiffness constants for the elastic elements and the torsional springs are calculated for static equilibrium using the experimental data for six motion types (flexion/extension, right/left torque, right/left bending). The static equilibrium equations, Eqs. (1) and (4), for all vertebrae (30 equations total) are solved simultaneously numerically. The static equilibrium problem is converted into a multiobjective optimization problem by minimizing the equilibrium equations for each vertebra. The rotation angles for each vertebra for all six motion types and four different external moment values (2.5, 5.0, 7.5 and 10.0 Nm) are known [13]. The stiffness constants are calculated

**Table 2 Nonlinear stiffness constants for flexion**

Vertebra	External Moment (Nm) <sup>a</sup>	$k_{sx}$ (Nm/rad)	$k_{sy}$ (Nm/rad)	$k_{sz}$ (Nm/rad)	$k_{srf}$ (N/m)	$k_{sif}$ (N/m)	$k_{irf}$ (N/m)	$k_{ijf}$ (N/m)
L5	2.50	36.40	0.00	0.00	390.26	386.46	0.77	0.75
	5.00	27.88	0.00	0.00	376.52	373.70	1.44	1.32
	7.50	26.53	0.00	0.00	271.03	274.90	1.17	48.26
	10.00	24.08	0.00	0.00	350.54	350.54	1.48	1.48
L4	2.50	0.00	0.00	0.00	418.41	418.47	390.26	386.46
	5.00	0.01	0.00	0.00	353.15	347.99	376.52	373.70
	7.50	0.00	0.00	0.00	241.43	238.49	271.03	274.90
	10.00	0.03	0.00	0.00	257.88	257.88	350.54	350.54
L3	2.50	0.00	0.00	0.00	178.34	172.89	418.41	418.47
	5.00	0.13	0.00	0.00	113.76	111.09	353.15	347.99
	7.50	0.00	0.00	0.00	65.50	40.42	241.43	238.49
	10.00	0.00	0.00	0.00	48.21	48.21	257.88	257.88
L2	2.50	0.01	0.00	0.00	10.63	10.74	178.34	172.89
	5.00	0.06	0.00	0.00	0.07	0.00	113.76	111.09
	7.50	0.00	0.00	0.00	1.10	1.11	65.50	40.42
	10.00	0.04	0.00	0.00	1.08	1.08	48.21	48.21
L1	2.50	75.26	0.00	0.00	0.00	0.00	10.63	10.74
	5.00	102.03	0.00	0.00	0.00	0.00	0.07	0.00
	7.50	122.56	0.00	0.00	0.00	0.00	1.10	1.11
	10.00	139.47	0.00	0.00	0.00	0.00	1.08	1.08

<sup>a</sup>X component of the external moment. Y and Z components are all zero for flexion motion.

155 for each externally applied moment. Due to space limitations,  
 156 solved stiffness constants only for flexion are presented in Table 2.  
 157 The results for the remaining motion types can be found in  
 158 Ref. [14].

After obtaining the stiffness constants at available loading conditions, curve fitting is applied to calculate stiffness values for any moment (not limited to the discrete experimental data). This curve fitting is based on a third degree polynomial:

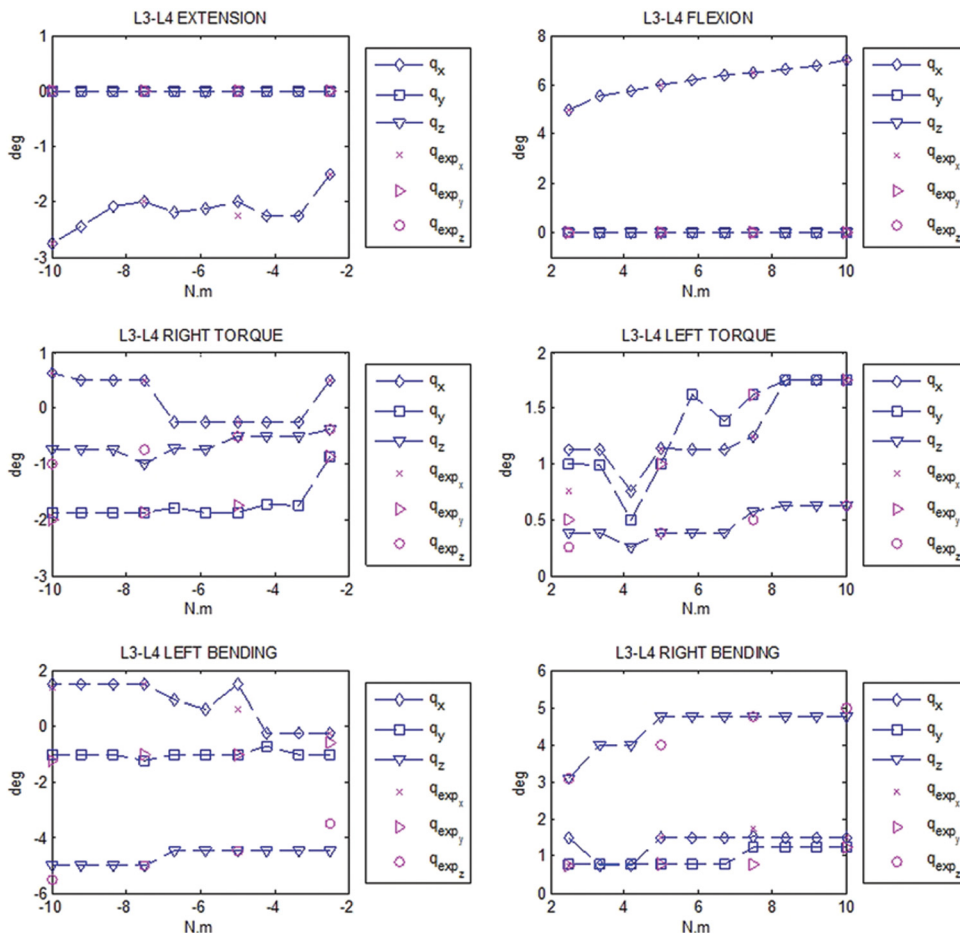


**Fig. 4 Model versus experimental data (L3-L4 shown)**

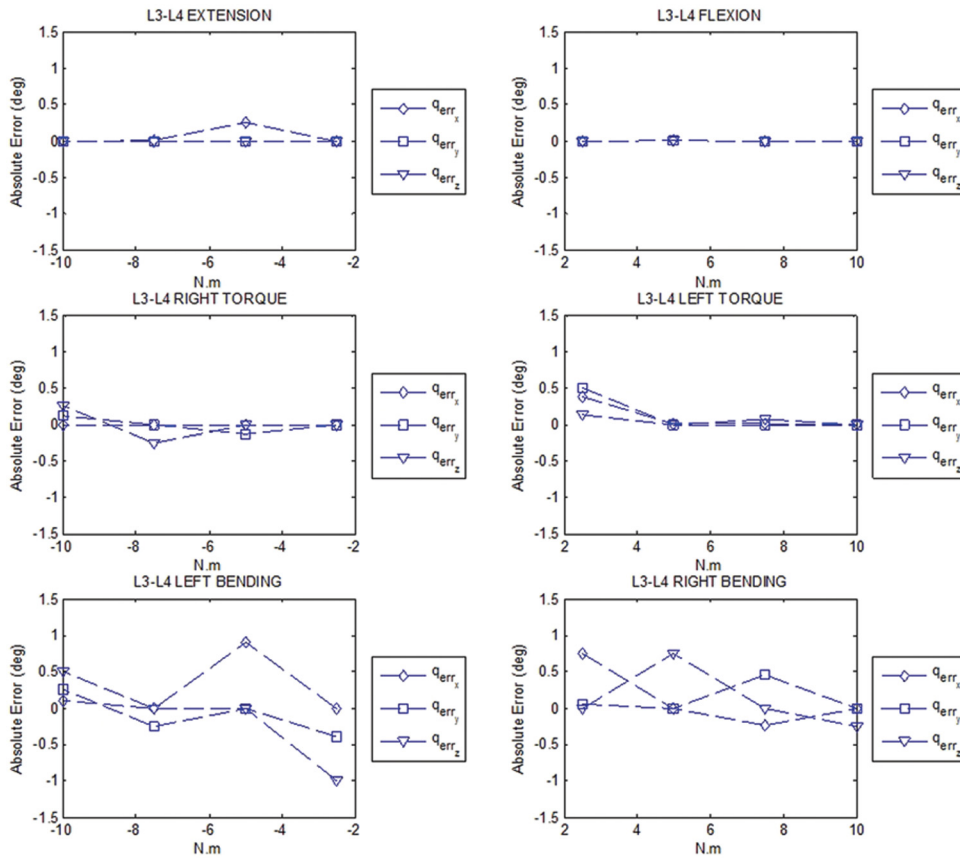


Fig. 5 Absolute error in model estimation of the experimental data (L3-L4 shown)

$$k = a * M_{ext}^3 + b * M_{ext}^2 + c * M_{ext} + d \quad (5)$$

163 k is the stiffness constant ( $k_{sx}$ ,  $k_{sy}$ ,  $k_{sz}$  for torsional springs or  $k_{sif}$ ,  
 164  $k_{sif}$ ,  $k_{irf}$ ,  $k_{if}$  for elastic elements),  $M_{ext}$  is the nonzero component  
 165 of the moment vector applied to the uppermost vertebra L1, and a,  
 166 b, c and d are the polynomial coefficients.

167 The second stage of validation is the comparison of the model  
 168 and experimental data. The model is tested under moments 2.50,  
 169 3.35, 4.20, 5.00, 5.85, 6.70, 7.50, 8.35, 9.20 and 10.00 Nm using  
 170 the stiffness constants obtained in the first stage by using Eq. (5).  
 171 The validation moment values include the experimental data  
 172 moments. Figure 4 shows the model output for the L3-L4 seg-  
 173 ment. The model closely follows the angle values for common  
 174 moment values tested, i.e., 2.5, 5.0, 7.5 and 10 Nm, typical of all  
 175 our results.

176 Figure 5 shows the absolute errors between the angles of rota-  
 177 tion predicted by the model and experimental data for the L3-L4  
 178 segment.

179 **4 Discussion**

180 A mathematical model that is validated by comparing its results  
 181 to experimental data becomes a powerful tool since the change of  
 182 parameters would be sufficient to modify a specific configuration  
 183 or a loading condition without repeating the experiment. The  
 184 purpose of this study was to create a tool to predict normal  
 185 anatomically-correct movement patterns for the human lumbar  
 186 spine. The proposed model, as seen from the results, closely fol-  
 187 lows the experimental data when they are available and predicts  
 188 the movement patterns for six different motion types continuously  
 189 for applied moment within 0–10 Nm.

190 The experimental or model data relating to the motion of the  
 191 spine varies from specimen to specimen [15]. For instance, when  
 192 the same motion model is tested with ligament stiffness values

193 chosen from different experimental studies, the intersegmental  
 194 rotation (L3-L4) results are significantly affected [16]. This vari-  
 195 ability makes it even harder to compare results. In this model, the  
 196 effect of the ligaments of the spine except for the facet capsulary  
 197 ligaments was incorporated into three parameters (stiffness values  
 198 of the torsional springs). To the authors' knowledge, this aspect of  
 199 the proposed model has not been employed in the literature. It is  
 200 also noted that all parameters can be calculated for specific experi-  
 201 mental data using the method detailed in this study. When using  
 202 this method, care must be taken in terms of the placement of the  
 203 spherical joints since that location must match the origin of the  
 204 coordinate system with respect to which the experimental data  
 205 were measured. The predicted response is sensitive to this location  
 206 and may require additional effort to locate accurately [10].

207 Though this model was derived to acquire anatomically-correct  
 208 motion patterns for a robotic spine, it is general for other pseudo-  
 209 static lumbar spine biomechanical applications. For example,  
 210 the model predicts the displacement of any point on any lumbar  
 211 vertebra, useful in studies of lumbar spine muscles length  
 212 changes.

213 There are limitations to the model. First, this model would  
 214 not be reliable for motions with high accelerations, which require  
 215 inertial forces, ignored in the proposed model and the referenced  
 216 experimental data. Second, combined motion of the lumbar spine  
 217 is not addressed in this model, requiring application of external  
 218 moments about more than one axis. Accelerated and/or combined  
 219 motions are seldom utilized during clinical diagnoses. The results  
 220 are satisfactory for programming the RLS since it targets training  
 221 medical students.

222 The palpation of muscles and soft tissue is significant for  
 223 palpatory diagnosis. The forces of the spinal muscles can be incor-  
 224 porated into the model applying a force generation model and  
 225 considering the attachment points on the bones and tendons. How-  
 226 ever, deciding how the muscles would “feel” like (when touched

227 by a physician) between those attachment points would be a quite  
 228 involved task. The ultimate goal of this model was to produce the  
 229 angles of rotations to be commanded to the robotic lumbar spine  
 230 as realistically as possible. Upon building the robotic lumbar  
 231 spine, the addition of the muscles and soft tissue will be per-  
 232 formed with strong collaboration of the faculty from the College  
 233 of Osteopathic Medicine at Ohio University. We have been work-  
 234 ing with DOs for a long time in matters that require their feedback  
 235 in terms of how normal or dysfunctional tissue would feel like. In  
 236 the past, we have had success in developing virtual training simu-  
 237 lations using their valuable feedback.

238 The RLS will be programmed to be controlled by a force-  
 239 feedback joystick. Via joystick motion, the angles of rotations  
 240 from this study will be commanded to the RLS, representing nor-  
 241 mal lumbar spine movement. Abnormalities from known dysfunc-  
 242 tional movement patterns will also be enabled.

243 In conclusion, a three-dimensional mathematical model to esti-  
 244 mate the normal movement patterns of the lumbar spine under dif-  
 245 ferent loading conditions was proposed. This model will be used  
 246 in programming of a cable-actuated Robotic Lumbar Spine for  
 247 training of medical students to identify normal and abnormal  
 248 movement patterns. Model parameters were obtained by using  
 249 previously-published experimental data and results validation  
 250 showed good agreement.

### References

- 251 [1] Karadogan, E., and Williams, R. L., II, 2010, "A Cable-Actuated Robotic Lum-  
 252 bar Spine for Palpatory Training of Medical Students," CD Proceedings of the  
 253 ASME International Design Technical Conferences, 34th Mechanisms and  
 254 Robotics Conference, Montreal, Quebec, Canada, Aug. 15–18, Paper No.  
 255 DETC2010-28863.  
 256 [2] Panjabi, M. M., 1973, "Three-Dimensional Mathematical Model of the Human  
 Spine Structure," *J. Biomech.*, **6**, pp. 671–680.  
 [3] Soni, A. H., Sullivan, J. A., Jr., Patwardhan, A. G., Gudavalli, M. R., and Chit-  
 wood, J., 1982, "Kinematic Analysis and Simulation of Vertebral Motion Under

- Static Load – Part I: Kinematic Analysis," *J. Biomech. Eng.*, **104**(2), pp. 257  
 105–111. 258  
 [4] Lavaste, F., Skalli, W., Robin, S., Roy-Camille, R., and Mazel, C., 1992,  
 "Three-Dimensional Geometrical and Mechanical Modeling of the Lumbar 259  
 Spine," *J. Biomech.*, **25**, pp. 1153–1164. 260  
 [5] Cheng, C., and Kumar, S., 1991, "A Three-Dimensional Static Torso Model  
 for the Six Human Lumbar Joints," *Int. J. Indust. Ergonomics*, **7**, pp. 261  
 327–339. 262  
 [6] Case, K., Xiao, D., Acar, B. S., and Porter, J. M., 1999, "Computer-Aided Mod-  
 eling of the Human Spine," *Proc. Inst. Mech. Eng.*, **213**, pp. 83–86. 263  
 [7] Cholewicki, J., Crisco, J. J., Oxland, T. R., Yamamoto, I., and Panjabi, M. M.,  
 1996, "Effects of Posture and Structure on Three-Dimensional Coupled Rotations  
 in the Lumbar Spine. A Biomechanical Analysis," *Spine*, **21**(21), pp. 264  
 2421–2428. 265  
 [8] Belytschko, T. B., Andriacchi, T. P., Schultz, A. B., and Galante, J. O., 1973,  
 "Analog Studies of Forces in the Human Spine: Computational Techniques," *J.*  
*Biomech.*, **6**(4), pp. 361–371. 267  
 [9] Schultz, A. B., Belytschko, T. B., Andriacchi, T. P., and Galante, J. O., 1973,  
 "Analog Studies of Forces in the Human Spine: Mechanical Properties and  
 Motion Segment Behavior," *J. Biomech.*, **6**(4), pp. 373–383. 269  
 [10] Patwardhan, A. G., Soni, A. H., Sullivan, J. A., Jr., Gudavalli, M. R., and Sriniv-  
 asan, V., 1982, "Kinematic Analysis and Simulation of Vertebral Motion  
 Under Static Load – Part II: Simulation Study," *J. Biomech. Eng.*, **104**(2), pp. 271  
 105–111. 272  
 [11] Sullivan, J. A., Soni, A. H., and Patwardhan, A. G., 1979, "Kinematic Analysis  
 of Intervertebral Motion of the Human Lumbar Spine," OREF (to be  
 published). 274  
 [12] Sharma, M., Langrana, N. A., and Rodriguez, J., 1998, "Modeling of Facet  
 Articulation as a Nonlinear Moving Contact Problem: Sensitivity Study on  
 Lumbar Facet Response," *J. Biomech. Eng.*, **120**(1), pp. 118–125. 276  
 [13] Panjabi, M. M., Oxland, T. R., Yamamoto, I., and Crisco, J. J., 1994,  
 "Mechanical Behavior of the Human Lumbar and Lumbosacral Spine as Shown  
 by Three-Dimensional Load-Displacement Curves," *J. Bone Jt. Surg., Am.*, **76**,  
 pp. 413–424. 278  
 [14] Karadogan, E., 2011, "A Cable-Actuated Robotic Lumbar Spine as the Haptic  
 Interface for Palpatory Training of Medical Students," Ph.D. thesis, Ohio Uni-  
 versity, Athens, OH. 279  
 [15] Adams, M. A., Hutton, W. C., and Stott, J. R. R., 1980, "The Resistance to  
 Flexion of the Lumbar Intervertebral Joint," *Spine*, **5**, pp. 245–253. 283  
 [16] Zander, T., Rohlmann, A., and Bergmann, G., 2004, "Influence of Ligament  
 Stiffness on the Mechanical Behaviour of a Functional Spinal Unit," *J. Bio-  
 mech.*, **37**, pp. 1107–1111. 284  
 285

AQ1

AQ2

Author Proof